

An Analytical Small-Signal Bias-Dependent Non-Uniform Model for *p-i-n* Traveling-Wave Photodetectors

G. Torrese^{*}, I. Huynen^{*}, M. Serres^{*}, D. Gallagher⁺, M. Banham⁺,
and A. Vander Vorst^{*}

* Microwave Laboratory

Université catholique de Louvain-la-Neuve (UCL)

Louvain-la-Neuve, Belgium.

E-mail:torrese@emic.ucl.ac.be

Fax: +32-10478705

⁺ Photon Design, Oxford, UK

email: dfgg@photond.com

Fax: +44-1865-395481

Abstract

A fully-analytical small-signal model is developed for the frequency response of traveling-wave photodetectors (TWPD). It takes into account the dependence of the equivalent transmission line admittance on the position, induced by the non-uniform distribution of the optical beam along the traveling direction. Moreover, the influence of the bias voltage on the transit time has been accurately investigated. The model is applied to the design of a InAlAs/InGaAs *p-i-n* photodetector. Its performances are investigated in term of electrical bandwidth.

Keywords

Index Terms – Traveling-wave photodetector, bandwidth, saturation regime

I. INTRODUCTION

IN the last years interest for high-speed traveling-wave photodetectors has increased [1], [2], [3]. These devices are expected to play an important role in the optical communication field because, unlike vertically-illuminated *p-i-n* photodiodes (VPDs), they can achieve a large bandwidth-efficiency product. As a matter of fact, to increase the VPD bandwidth the carrier transit time must be minimized, while a thick intrinsic region is necessary for light absorption [4]. Moreover, traditional *p-i-n* photodiodes are limited by a RC time constant. The general outline of traveling-wave photodiodes (TWPDS) consists of an electrical coplanar transmission line coupled to an optical waveguide. The electrical field is applied perpendicular to the photon path, hence bandwidth and internal quantum-efficiency can be optimized separately. If matching condition between the optical and the electrical signal traveling along the photodetector is achieved, the usual RC time constant cannot be defined and the main limit on the bandwidth is due to reflections at the input and output ends of the structure. As discussed in [2], propagation on TWPDS is quasi-TEM. Transmission line equivalent circuits describing the properties of quasi-TEM waveguides have been extensively investigated in literature [2], [3]. It should however be noted that, both the impedance and the shunt admittance of these proposed equivalent circuits, not only are independent of the light source characteristics but also of the external reverse voltage used to bias the photodetector. Another important feature of *p-i-n* devices is that the junction transit time generally depends on the reverse voltage. Although the

basic theory on traveling-wave solid-state device has been previously published by Soohoo *et al.* [5] it applies to simple case when detectors operate at electric field large enough to saturate the carrier velocity. The same hypothesis has been utilized by Huynen *et al.* in [6] and [7]. Moreover, results provided in [7] have been obtained by neglecting the influence of the transit time.

The small-signal model presented in this paper takes into account the non-uniformity of the shunt distributed admittance of the line, induced by the exponential decrease of light power along the optical traveling path, and the influence on the transit time of the bias voltage, enabling to predict the TWPD behavior in both saturated and unsaturated regime. In the next section, we present in detail the distributed equations for investigating the behavior of TWPDs. We formally derive an expression for the current density, and we obtain a RF transmission line model depending on the loads at input and output ends of the device. In section III we optimize the TWPD geometry for optical conversion. Section IV illustrates the efficiency of the model by comparison with simulations using previously published models.

II. TWPD MODEL

A. Determination of the small-signal current

In order to investigate the behavior of TWPDs we divide the photodetector into differential sections of length Δz , and then we determine for each section the total current density as sum of drift and displacement components. Essentially the total current density is calculated from a one-dimensional model in the x-direction. The whole device is obtained by repeating n times a section in the z -direction, as for traditional transmission

lines. If a section is sufficiently short, we can consider that the absorbed light is constant.

Assuming no back-reflection at the end of structure, the optical generation rate is

$$G(z, t) = G_0 + G_a(e^{-(\alpha_o + j\beta_o)z + j\omega t}) \quad (1)$$

where the optical absorption coefficient α_o and the propagation coefficient β_o are defined according to [6]. In (1) ω is the RF angular frequency, while G_0 and G_a represent the signal amplitude of the DC and AC components, respectively. As we consider a side illumination with uniform distribution in $x - y$ plane, the generation term $G(z, t)$ is x - and y -independent.

In order to determine the total current density a perturbational approach [8] has been used to solve the transport equations. We assume that all variables can be written as the sum of a DC or time-average part and an AC or time-dependent part. Further, in agreement with the small-signal analysis, it is assumed that the AC quantities are very small in comparison with the DC ones. These hypotheses allow us to decouple the transport equations into 0^{th} - and 1^{st} -order equations, then the DC or non perturbational equations are solved first. As shown in [9], when considering a constant electric field *vs.* the $x - y$ section of the intrinsic region, and when neglecting the carrier recombination, the total current density can be determined in an analytical fashion. To derive the analytical closed-form for the current density we also neglected the charge trapping mechanism although it should be taken into account for accurate modeling. The DC and AC current densities are, respectively,

$$J_0(x, z) = qE_0(n_0\mu_{n0} + p_0\mu_{p0}) \quad (2)$$

and

$$J_a(x, z) = j\omega\epsilon_s E_a + q((E_a(n_0\mu_{n0} + p_0\mu_{p0}) +$$

$$E_0(n_a\mu_{n0} + n_0\mu_{na} + p_a\mu_{p0} + p_0\mu_{pa})) \quad (3)$$

where n and p represent the electron and hole carrier densities, respectively, μ_n and μ_p the electron and hole mobilities, E the electric field, q the electron charge and ϵ_s the material permittivity, while the indices 0 and a indicate the unperturbed (DC) and perturbated (AC) variables, respectively. Expressions (2) and (3) are very similar to those in [9], exception made that carrier densities and electric fields are now z-dependent, because of the optical generation rate (1). In (2) and (3) the transit time is taken into account, since carrier mobilities appear. Also, the used mobility model depends on the electric field. Consequently our model allows us to simulate p - i - n devices outside the saturation regime. Now, integrating equation (3) with respect to the x variable between 0 and d , and multiplying by (w/d) , the AC current can be rewritten as

$$I_a = \frac{w}{d} \int_0^d J_a(x) dx = -Y_a V_a + (w/d) B e^{-z(\alpha_o + j\beta_o)} \quad (4)$$

where d is the thickness of the intrinsic region, w the width of the photodetector while the admittance per-unit-length Y_a (S/m) is given by

$$Y_a = (w/d) (A e^{-\alpha_o z} + j\omega \epsilon_s) \quad (5)$$

while the A and B terms result:

$$A = \frac{q\alpha_o \eta_i P_o}{2S h \nu E_0 \mu_{n0} \omega^2 \mu_{p0}} (A_1 + A_2 + 2(A_3 + A_4)/d) \quad (6)$$

$$B = -\frac{E_0 q \alpha_o \eta_i P_a}{S h \nu \omega^2} B_1 \quad (7)$$

with coefficients $A_1 - A_4$ and B_1 given in Appendix A. In (6) and (7) P is the incident optical power, S the illuminated surface, η_i the internal quantum-efficiency, h the Planck's

constant and ν the optical frequency. The term B represents the distributed current source due to the photogeneration process. It should be noted that, when no light is applied, both A and B are zero, so that the AC current is only due to the displacement mechanism.

B. Non-uniform Transmission Line Model

As shown in [2], waves propagating along TWPD are characterized by electric and magnetic field that are quasi-transverse. As only the x -component of the AC electric field is taken into account for each section, we can assume that $E_y = E_z \approx 0$ and that no variation of the E_x component occurs in the y-direction. Hence, by noting that the current flows only in the x -direction, the time-harmonic form of the two curl Maxwell's equations can be combined into

$$\frac{\partial E_x^2}{\partial^2 z} - j\omega\mu_s J_a(x, z) = 0 \quad (8)$$

Thus the traveling-wave photodetector behavior can be completely determined once that we know the current density $J_a(x)$. Integrating equation (8) in the x -direction and using (4) yields a second-order linear non-homogeneous differential equation which is solved for the small-signal voltage $V_a(z)$ as a function of an optical power dependent source term

$$\frac{\partial V_a^2}{\partial^2 z} - \gamma_{rf}^2 V_a = -Z_a B \frac{w}{d} e^{-(\alpha_o + j\beta_o)z} \quad (9)$$

where the complex propagation coefficient γ_{rf} and characteristic impedance Z_c are

$$\gamma_{rf}(z) = \sqrt{Z_a Y_a(z)} \quad \text{and} \quad Z_c(z) = \sqrt{\frac{Z_a}{Y_a(z)}} \quad (10)$$

with an impedance per-unit-length (Ω/m)

$$Z_a = \frac{j\omega\mu_s d}{w} \quad (11)$$

As shown by formula (5), the admittance per-unit-length Y_a is position dependent, unless no light is applied. On the other hand, the impedance per-unit-length Z_a can be assumed position independent as the light effect does not largely affect its value. It can be determined as suggested in [2], although a full-wave analysis is required for rigorous modeling [10]. The solution of the differential equation (9) has been determined analytically by the method of variation of parameters, although a more elegant solution can be found by using the Green's function technique as done by Soohoo *et. al* in [5]. However, in comparison with results provided in [5], the solution of equation (9) is more complex, because of non-uniformity of the transmission line. Finally, the solution of (9) depends on two unknowns constants which are fixed by applying the following conditions at the two ends of the TWPD:

$$\frac{I_a(0)}{V_a(0)} = Y_o \quad \text{and} \quad \frac{I_a(L)}{V_a(L)} = -Y_L \quad (12)$$

where Y_o and Y_L are the admittance of the ending loads at the input and output of the device respectively.

III. OPTICAL DESIGN

The model presented in the previous section can be used for device optimization. Fig. 1 shows the intensity field profile of the fundamental TE optical mode obtained by using the software Fimmwave from Photon Design together with the cross-section of the TWPD optimized for $1.33 \mu\text{m}$ operation. The intrinsic region has been designed by sandwiching a high refractive $In_{0.53}Ga_{0.47}As$ region between two $In_{0.52}Al_{0.48}As$ layers. By adjusting the active layer thickness, the confinement factor is tailored to concentrate the field inside the intrinsic region while a single quantum well with a large absorption coefficient allows

to absorb the optical radiation in a few microns. The Fimmwave simulation yields an effective modal index of 3.512 in the intrinsic region by using a rigorous fully vectorial solution of Maxwell's equations.

IV. RESULTS

Fig. 2 shows the output current frequency response for four different values of the optical absorption coefficient α_o : $10^3, 3 \times 10^3, 10^4$ and $10^5 m^{-1}$. The photodetector has been left open at the input end ($Y_o = 0$) and the output end has been matched to the characteristic impedance ($Y_L = Y_c$). Curves have been traced by using two different models: solid lines show results obtained with the present model, while dashed ones come from a combination of previously published models [6], [7]. They use simplified equations for the carrier motion within the intrinsic region [6]. Despite of the fact that the dashed model assumes no z -dependence of the distributed characteristic impedance and propagation constant, and is valid in saturation regime only, an excellent agreement is observed between the two models. This is because the bias voltage V taken equal to 10 volts is sufficient to saturate the μ_n and μ_p carrier mobilities. Moreover, we used an extremely low optical power P_a , in order to avoid nonlinear saturation effects. Consequently, the z -dependent term in expression (5) is 13 orders of magnitude less than the uniform term. Under these assumptions the small discrepancies between solid and dashed lines have to be attributed to the different models used for the carrier motion in the $p-i-n$ junction. Fig. 2 also shows that for values of α_o equal or greater than $10^4 m^{-1}$, the light absorption is total, since photogenerated current for those values converge at low frequencies. The bandwidth is maximal for the highest value of α_o , because the distributed photogenerated current concentrates at the

input of the TWPD. Thus, the bandwidth limitation due to phase mismatch between forward distributed photogenerated current waves and reverse ones generated at the open end is reduced [7]. Hence, for $\alpha_o = 10^5 m^{-1}$, the device response is only limited by the carrier transit time.

Fig. 3 illustrates the influence on the bandwidth of the thickness d of the intrinsic area, and of the mismatch between the output load and the characteristic impedance. It first compares the matched output-end frequency response for $d = 0.2\mu m$ (-.) and for $d = 1.0\mu m$ (- -): the characteristic impedance depends on d , hence the output load Z_L is taken different for the two simulated curves to ensure matching. The model verifies that increasing the thickness of the intrinsic region reduces the bandwidth, because the carrier transit time increases. Solid lines show the current response obtained for $d = 0.2\mu m$, but with the output load impedance Z_L equal to the characteristic impedance for a $1\mu m$ -thick intrinsic region. Due to mismatch, a strong ripple occurs in the frequency response.

Fig. 4 illustrates the influence on the bandwidth of the biasing voltage V . First, varying the voltage from $5V$ (curve -.) down to $0.1V$ (curve - -) increases the bandwidth. This shows the sensitivity of the model to the bias conditions of the $p-i-n$ junction. Finally, solid curve (-) shows the frequency response of lumped photodetector of same cross-section, illuminated in a similar way: in this case, the junction capacitance effect predominates, which reduces the bandwidth, compared to the TWPD operation mode (-.).

V. CONCLUSIONS

This paper has presented a fully-analytical non-uniform model for analyzing the bandwidth of $p-i-n$ TWPDs. The model shows first that the non uniformity in the distributed

admittance has no significant influence. Also, it enables to optimize the bandwidth and quantum-efficiency of the device, by adjusting the absorption coefficient, the geometry of the intrinsic region, the output load impedance, and the bias voltage.

APPENDIX

$$A_1 = ((-\beta_p E_0 - 2 \mu_{p0}) \mu_{n0} - \beta_n E_0 \mu_{p0}) \omega^2 d \quad (13)$$

$$A_2 = 2 j \mu_{p0} \mu_{n0} \omega E_0 ((\beta_p + \beta_n) E_0 + (\mu_{n0} + \mu_{p0})) \quad (14)$$

$$A_3 = \left(-e^{\frac{j\omega d}{E_0 \mu_{n0}}} + 1 \right) \mu_{p0} E_0^2 \mu_{n0}^2 (\mu_{n0} + E_0 \beta_n) \quad (15)$$

$$A_4 = \left(1 - e^{\frac{j\omega d}{E_0 \mu_{p0}}} \right) \mu_{n0} \mu_{p0}^2 E_0^2 (\beta_p E_0 + \mu_{p0}) \quad (16)$$

$$B_1 = \left(\left(1 - e^{\frac{j\omega d}{E_0 \mu_{p0}}} \right) \mu_{p0}^2 + \left(1 - e^{\frac{j\omega d}{E_0 \mu_{n0}}} \right) \mu_{n0}^2 \right) \quad (17)$$

$$E_0 + j\omega d(\mu_{n0} + \mu_{p0})$$

and

$$\beta_{n,p} = \frac{d\mu_{n,p}}{dE} \Big|_{E=E_0} \quad (18)$$

ACKNOWLEDGMENTS

This research has been funded by the PAI-IV/13 project of the Belgian Federal Office for Scientific, Technical and Cultural Affairs. Acknowledgments are also due to the National Fund for Scientific Research, Belgium and to the Ministry of Education of the Grand Duchy of Luxembourg, who partially funded this research.

REFERENCES

- [1] K. Giboney, R. Nagarajan, T. Reynolds, S. Allen, R. Mirin, and M. Rodwell, "Traveling-wave photodetectors with 172-GHz bandwidth-efficiency product," *IEEE Photon. Technol. Lett.*, vol. 7, no. 4, pp. 412–414, Apr. 1995.
- [2] K.S. Giboney, M.J.W. Rodwell, and J.E. Bowers, "Traveling-wave photodetectors theory," *IEEE Trans. Microwave Theory Tech.*, vol. 45, pp. 1310–1319, Aug. 1997.
- [3] V.M. Hietala, G.A. Vawter, T.M. Brennan, and B.E. Hammons, "Traveling-wave photodetectors for high-power large-bandwidth applications," *IEEE Trans. Microwave Theory Tech.*, vol. 43, pp. 2291–2298, Sep. 1995.
- [4] J.E. Bowers and C.A. Burrus Jr., "Ultrawide-band long wavelength p-i-n photodetectors," *Journal Lightwave Technol.*, vol. 5, pp. 1339–1350, Oct. 1987.
- [5] J. Soohoo, S.-K. Yao, J.E. Miller, R.R. Shurtz II, Y. Taur, and R.A. Gudmundsen, "A laser-induced traveling-wave device for generating millimeter waves," *IEEE Trans. Microwave Theory Tech.*, vol. 29, no. 11, pp. 1174–1182, Nov. 1981.
- [6] I. Huynen, A. Salamone, and M. Serres, "A traveling-wave model for optimizing the bandwidth of p-i-n photodetectors in silicon-on-insulator technology," *IEEE J.Sel. Topics Quantum Electron.*, vol. 4, no. 6, pp. 953–963, Nov.–Dec. 1998.
- [7] I. Huynen and A. Vander Vorst, "A 4-port scattering matrix formalism for p-i-n traveling wave photodetectors," *IEEE Trans. Microwave Theory Tech.*, vol. 48, no. 6, pp. 1007–1016, Jun. 2000.
- [8] S.E. Laux, "Techniques for small-signal analysis of semiconductor devices," *IEEE Trans. Electron Devices*, vol. ED-32, pp. 2028–2037, Oct. 1985.
- [9] G. Torrese, A. Salamone, I. Huynen, and A. Vander Vorst, "A fully analytical model to describe the high-frequency behavior of p-i-n photodiodes," *Microwave and Optical Technology Letters*, vol. 31, no. 5, pp. 329–333, Dec. 2001.
- [10] T. Shibata and E. Sano, "Characterization of MIS structure coplanar transmission lines for investigation of signal propagation in integrated circuits," *IEEE Trans. Microwave Theory Tech.*, vol. 38, no. 7, pp. 881–890, Jul. 1990.

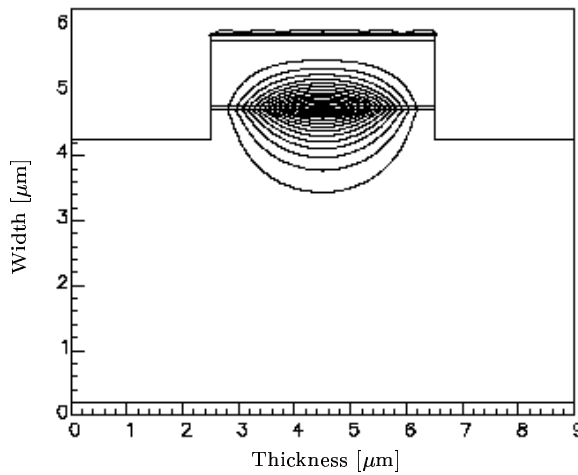


Fig. 1. 2D view of traveling-wave topology analyzed using Fimmwave software. Lines show contour of equal optical intensity. Geometrical parameters are: thickness of intrinsic area $d=0.87 \mu\text{m}$, width of mesa structure $w=4 \mu\text{m}$, section $S=w d$. Optical refraction index computed by Fimmwave is $n_{eff}=3.512$.

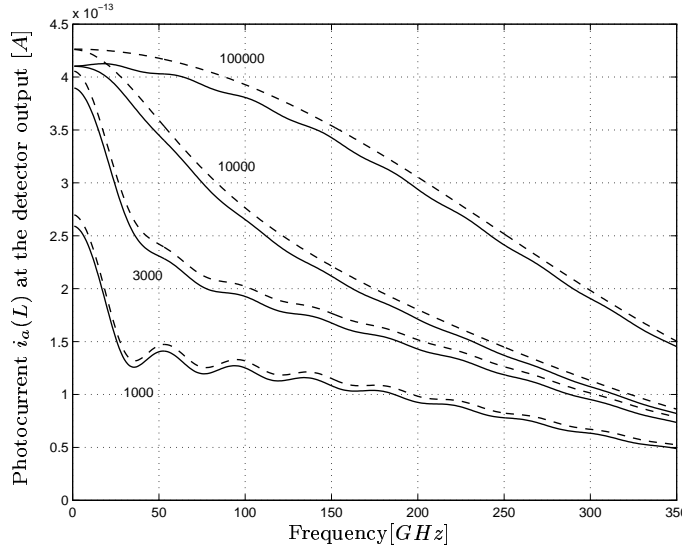


Fig. 2. Output current of input open-ended TWPD ($Y_o = 0$, $Y_L = 1/Z_c = 1/(7.18 \Omega)$) for four different values of optical absorption coefficient. Geometrical parameters are: $d = 0.2 \mu\text{m}$, $w = 3 \mu\text{m}$, length $L = 1 \text{ mm}$. Electrical and optical parameters are $n_{opt} = n_{rf} = 3.5$, optical wavelength $\lambda_{opt} = 1.06 \mu\text{m}$, AC modulation of optical power $P_{ac} = 0.001 \text{ nW}$, bias voltage $V = 10 \text{ V}$. Solid lines are for present model, while dashed ones correspond to model presented in [6].

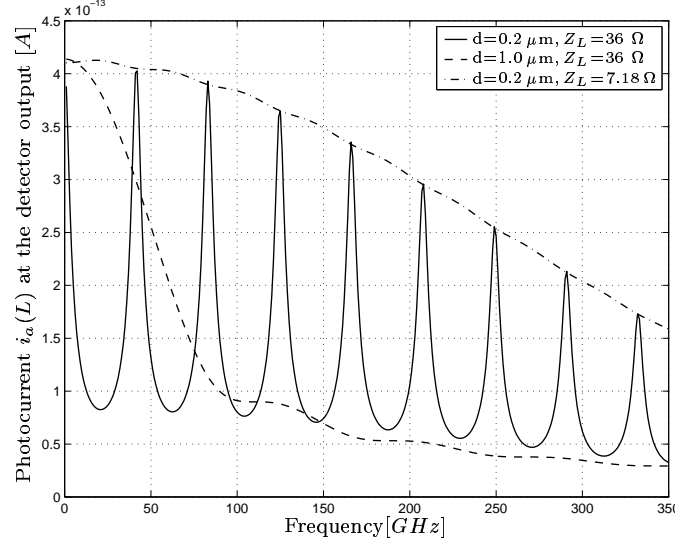


Fig. 3. Output current of input open-ended TWPD for three different combinations of intrinsic thickness d and output load Z_L : ($d = 0.2 \mu m$, $Z_c = Z_L = 7.18 \Omega$): curve (- -), ($d = 1.0 \mu m$, $Z_L = Z_c = 36 \Omega$): curve (- .), ($d = 0.2 \mu m$, $Z_c = 7.18 \Omega$, $Z_L = 36 \Omega$): curve (-). Geometrical parameters are: $w = 3 \mu m$, $L = 1 \text{ mm}$. Electrical and optical parameters are $n_{opt} = n_{rf} = 3.5$, $\lambda_{opt} = 1.06 \mu m$, $\alpha_o = 2 \times 10^6 m^{-1}$, $P_{ac} = 0.001 nW$, $V = 10 V$.

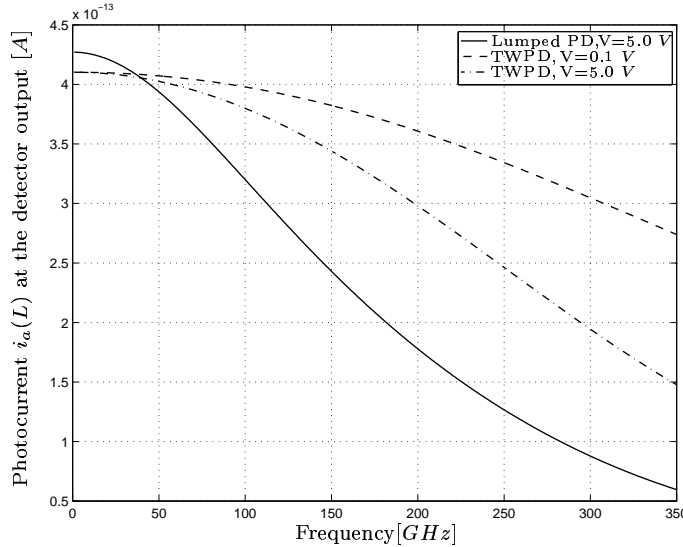


Fig. 4. Comparison between input open-ended TWPD ($Y_o = 0$, $Y_L = 1/Z_c = (1/7.18)$ S)) for two different values of bias voltage $V = 0.1$ V (- -), 5 V (-.), and side-illuminated lumped PD with $V = 5$ V (-). Geometrical parameters are: $d = 0.2$ μm , $w = 3$ μm , $L = 0.1$ mm. Electrical and optical parameters are $n_{opt} = n_{rf} = 3.5$, $\lambda_{opt} = 1.06$ μm , $\alpha_o = 10^5$ m^{-1} , $P_{ac} = 0.001$ nW .